A Single-Stage Inductive-Power-Transfer Converter for Constant-Power and Maximum-Efficiency Battery Charging

Zhicong Huang, *Member, IEEE*, Chi-Seng Lam, *Senior Member, IEEE*, Pui-In Mak, *Fellow, IEEE*, Rui Paulo da Silva Martins, *Fellow, IEEE*, Siu-Chung Wong, *Senior Member, IEEE*, and Chi K. Tse, *Fellow, IEEE*

***Abstract*—This article proposes a single-stage inductive-power-transfer (IPT) converter operating as a wireless constant-power (CP) and maximum-efficiency battery charger. By maintaining a constant output power rather than providing a constant output current throughout the dominant stage of battery charging, the IPT converter can make the utmost of its power capability, thus having a faster charging rate. The proposed single-stage IPT converter adopts series–series compensation and includes a switch-controlled capacitor (SCC) and a semiactive rectifier (SAR) in the secondary side. Manipulating the SCC and the SAR to emulate the optimum impedance of the resonator and the load, we propose a novel operation approach combining the merits of load-independent transfer characteristic and load impedance matching, to achieve a simple solution to CP charging and maximum efficiency throughout the charging process. Since the control scheme is based on fixed operating frequency and secondary-side real-time regulation, wireless feedback communication is not required. Moreover, soft switching and low voltage stress can be easily achieved in this IPT converter.**

***Index Terms*—Battery charging, constant power, inductive power transfer (IPT), maximum efficiency, soft switching.**

Manuscript received September 5, 2019; revised December 4, 2019; accepted January 21, 2020. Date of publication January 29, 2020; date of current version May 1, 2020. This work was supported in part by the Science and Technology Development Fund, Macao SAR (FDCT) under Projects 025/2017/A1 and SKL-AMSV Fund, and in part by the Research Committee of University of Macau under Projects MYRG2017-00090-AMSV and UM Macao Postdoctoral Fellowship. Recommended for publication by Associate Editor M. Ponce-Silva. *(Corresponding author: Zhicong Huang.)*

Z. Huang was with the State Key Laboratory of Analog and Mixed-Signal VLSI, University of Macau, Macao 999078, China. He is now with the Shien-Ming Wu School of Intelligent Engineering, South China University of Technology, Guangzhou 510006, China (e-mail: forward.huang@gmail.com).

C. S. Lam and P.-I. Mak are with the State Key Laboratory of Analog and Mixed-Signal VLSI, the Institute of Microelectronics, and the Department of Electrical and Computer Engineering, Faculty of Science and Technology, University of Macau, Macao 999078, China (e-mail: cslam@um.edu.mo; pimak@umac.mo).

R. P. da Silva Martins is with the State Key Laboratory of Analog and Mixed-Signal VLSI, the Institute of Microelectronics, and also with the Department of Electrical and Computer Engineering, Faculty of Science and Technology, University of Macau, Macao 999078, China (e-mail: rmartins@um.edu.mo).

S. C. Wong is with the Department of Electronic and Information Engineering, The Hong Kong Polytechnic University, Hong Kong (e-mail: enscwong@polyu.edu.hk).

C. K. Tse is with the Department of Electrical Engineering, City University of Hong Kong, Hong Kong (e-mail: cktse@ieee.org).

Color versions of one or more of the figures in this article are available online at https://ieeexplore.ieee.org.

Digital Object Identifier 10.1109/TPEL.2020.2969685

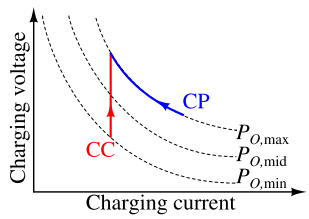

Fig. 1. *V–I* characteristics of CC charging and CP charging.

I. Introduction

INDUCTIVE power transfer (IPT) is a growing technology to wirelessly supply power in applications where physical connection is inconvenient or impossible, e.g., hostile environments being affected by dirt and moisture [1], [2]. Typically, with abilities to simplify charging operation and remove safety concerns associated with electrical connection, IPT converters are suitable for wireless battery charging in a variety of scenarios, such as mobile electronics, biomedical implants, small home appliances, and electric vehicles [3]–[7].

Thermal design for power electronics converters is mandatory [8]. In general, maximum extractable power of a power electronics converter is subject to practical thermal and physical constraints. Constant current (CC) charging is a common charging technique and a dominant charging process for widely used lithium-ion batteries [9]–[11]. As shown by the vertical CC line in Fig. 1, the charging current is kept constant, while the charging voltage is clamped to the terminal voltage of the battery and increases during charging. It can be observed that the charging power started with a minimum value and increased to a maximum value at the completion of CC charging. If CC charging is implemented, the IPT converter only delivers power at the maximum value for a very short duration near the completion of charging. Alternatively, to make the utmost of the power capability, the charger can control the output power to a predetermined maximum value and provide a constant-power (CP) charging for the battery [12]–[17], such that full-power delivery can be maintained throughout the whole charging process. As shown by the CP curve in Fig. 1, the charging current should be allowed to vary inversely with respect to the terminal voltage of

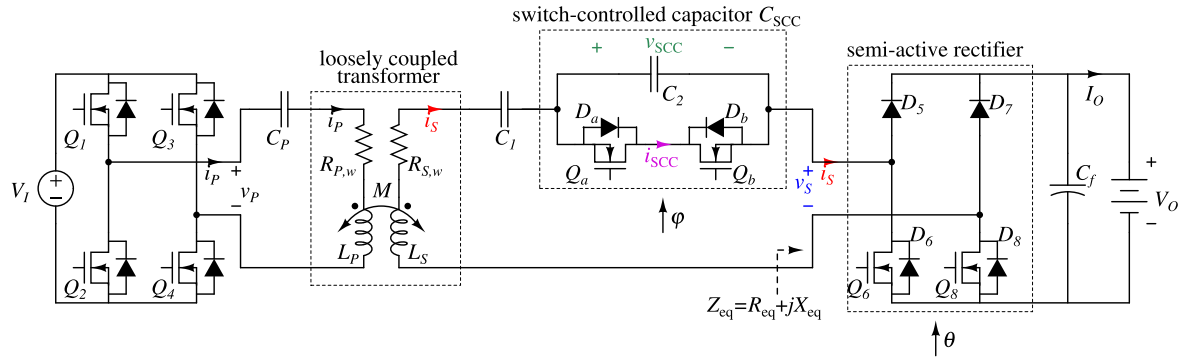

Fig. 2. Schematics of the proposed wireless CP charging system.

the battery to maintain the desired CP charging. Obviously, given an identical maximum charging power, CP charging provides a faster charging speed than that of CC charging [12]–[14]. Moreover, compared with CC charging, there is no problem of excessive thermal design with CP charging [15], [16].

For a conductive charger, it is relatively easy to facilitate CP charging in its battery management system, which operates the charger as a current source, constantly varying according to the charging power profile [12]–[17]. However, to our best knowledge, IPT converters with the ability of wireless CP charging are seldom explored in the literature, which motivates us to investigate the feasibility of the wireless CP charger. In general, an IPT converter should be designed to operate at some fixed operating frequencies with load-independent transfer characteristic for minimal control complexity and to operate within a restricted load range to achieve maximum efficiency [18]–[21]. However, only CC or constant voltage output is achievable at these fixed operating frequencies such that the output power of the IPT converter is determined by the load condition and cannot comply with the CP charging profile [22], [23]. An intuitive idea for CP output is using a two-stage IPT system, where a front-end converter can be used to modulate the input amplitude of the IPT converter or a load-side converter can be cascaded to the IPT converter for power regulation [24]–[27]. Due to the extra power stage, penalties of power loss, control complexity, and/or wireless feedback communication are inevitable. Moreover, keeping single-stage design in mind, the IPT converter should also have load matching ability to achieve high efficiency. Otherwise, the efficiency significantly degrades at some mismatched loading conditions [28]–[30]. Since the load range during battery charging is normally wide, it is difficult for a single-stage IPT converter to maintain the maximum efficiency, while permitting fixed operating frequency, soft switching, no extra cascading converter, and no wireless feedback communication [30]. Therefore, it is challenging for an IPT converter to achieve the required output for CP charging and maintain the maximum efficiency throughout the charging process.

Aimed at filling the gap of wireless CP charging, this article presents and explores a single-stage IPT converter which adopts series–series with a switched-controlled compensation capacitor (SCC) and a semiactive rectifier (SAR) in the secondary side. Combining the merits of load-independent transfer characteristic and load impedance matching, a novel operation approach is proposed for CP and maximum-efficiency charging. By controlling the SCC and the SAR, an optimum load and a constant secondary resonator current are maintained simultaneously, such that CP and maximum-efficiency charging can be simply implemented. The control scheme is based on fixed operating frequency and secondary-side real-time regulation, eliminating wireless feedback communication. Moreover, soft switching and low voltage stress can be easily achieved in this IPT converter.

II. Proposed Wireless CP Battery Charger

A. System Structure

Fig. 2 shows the proposed wireless CP battery charger based on a series–series compensated inductive power transfer (SSIPT) converter with an SCC and an SAR. In the schematic of the proposed system, the magnetic coupler has primary self-inductance L_P, secondary self-inductance L_S, and mutual inductance M. The coupling coefficient is defined as $k = \frac{M}{\sqrt{L_P L_S}}$. Coil losses in the primary and the secondary are represented by resistances $R_{P,w}$ and $R_{S,w}$, respectively. Both coils of the magnetic coupler are compensated by a capacitor in series connection. C_P is the primary compensation capacitor with fixed capacitance value, while a fixed-value capacitor C_1 as well as an SCC in series connection is used for secondary compensation with variable capacitance. The SCC consists of a fixed-value C_2 and two MOSFET switches Q_a and Q_b, with equivalent variable capacitance $C_{\rm SCC}$. D_a and D_b are the antiparallel body diodes of Q_a and Q_b, respectively. Compared with a single SCC, series connection of a fixed-value capacitor and an SCC can help to reduce the voltage stress of the SCC switches, which will be discussed in detail in Section IV-A. $v_{\rm SCC}$ is the voltage across the SCC, and $i_{\rm SCC}$ is the current flowing through the SCC. DC voltage source V_I is modulated into ac voltage v_P at an angular frequency ω to drive the primary coil by a full-bridge inverter with four MOSFET switches Q_1–Q_4. AC output is rectified to dc output by the SAR with output filter capacitor C_f. The SAR consists of two diodes D_5 and D_7 in the upper legs, and two MOSFET switches Q_6 and Q_8 in the lower legs. D_6 and D_8 are the antiparallel body diodes of Q_6 and Q_8, respectively. Secondary ac voltage v_S and ac current i_S are the inputs of the SAR circuit.

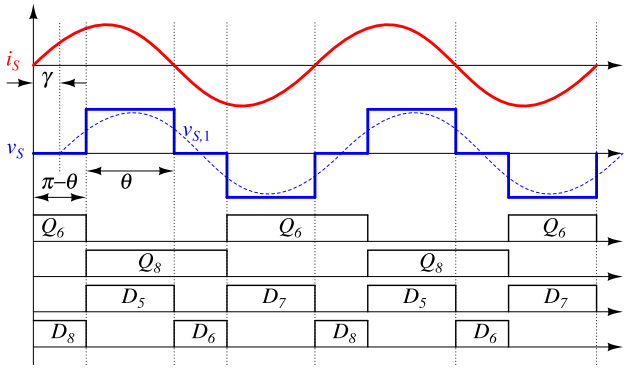

Fig. 3. Switching sequences and operating waveforms of the SAR.

V_O and I_O are dc charging voltage and current for the battery, respectively.

B. Operation of the SAR

The switching sequences and the operating waveforms of the SAR are shown in Fig. 3. MOSFET switches Q_6 and Q_8 are turned ON during the ON-time of their antiparallel diodes to have zero-voltage switching (ZVS). Both Q_6 and Q_8 are turned ON for half a cycle, and they are complements of each other. Then, Q_6 is turned OFF with a time delay of $\pi - \theta \in [0, \pi]$ to the zero-cross point where i_S commutates from negative to positive, while Q_8 is turned OFF with a time delay of $\pi - \theta \in [0, \pi]$ to the zero-cross point where i_S commutates from positive to negative. Thus, the conduction angle θ of the SAR has a maximum π and minimum 0. It is noted that the change of θ will affect the phase angle between v_S and i_S. As shown in Fig. 3, $v_{S,1}$ is the fundamental component of v_S that it lags i_S with a phase angle given by $\gamma = \frac{\pi-\theta}{2}$. Therefore, the equivalent load is an impedance instead of the usual pure resistance [30], [31].

Since the battery charging is a slow process compared with the operating period of the SSIPT converter, the battery is modeled as a resistor determined by charging voltage and charging current, i.e., $R_L = \frac{V_O}{I_O}$. It has been studied that the SAR together with the resistive load can be represented by an equivalent fundamental impedance [32], [33], given by

$$Z_{\text{eq}} = R_{\text{eq}} + jX_{\text{eq}} \tag{1}$$

where

$$R_{\text{eq}} = \frac{8}{\pi^2} R_L \sin^4\left(\frac{\theta}{2}\right) \text{ and} \tag{2}$$

$$X_{\text{eq}} = -\frac{8}{\pi^2} R_L \sin^3\left(\frac{\theta}{2}\right) \cos\left(\frac{\theta}{2}\right) \tag{3}$$

are equivalent resistance and capacitive reactance, respectively.

C. Operation of the SCC

The switching sequences and the operating waveforms of the SCC are shown in Fig. 4. Both Q_a and Q_b are turned ON for half a cycle, and they are complements of each other. Then, Q_a is turned ON with a time delay of $\varphi \in [\frac{\pi}{2}, \pi]$ to the zero-cross point where i_S commutates from negative to positive, while Q_b is turned ON with a time delay of $\varphi \in [\frac{\pi}{2}, \pi]$ to the zero-cross point where i_S commutates from positive to negative. Since Q_a and Q_b are turned ON at zero voltage, soft switching can be achieved to minimize the switching losses. The available charging time (or discharging time) for C_2 in half a cycle is $\pi - \varphi$, which decreases with the increase of φ and results in a small equivalent root-mean-square (rms) value of v_{SCC}. Consequently, the equivalent capacitance C_{SCC} of the SCC can be modulated by varying the control angle φ. It has been studied that C_{SCC} can be calculated by considering the fundamental components of i_S and v_{SCC} [34], [35]. The capacitive reactance donated by C_{SCC} is highlighted as

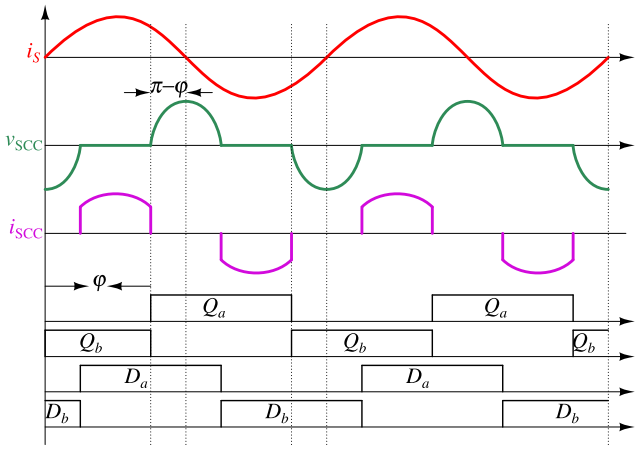

Fig. 4. Switching sequences and operating waveforms of the SCC.

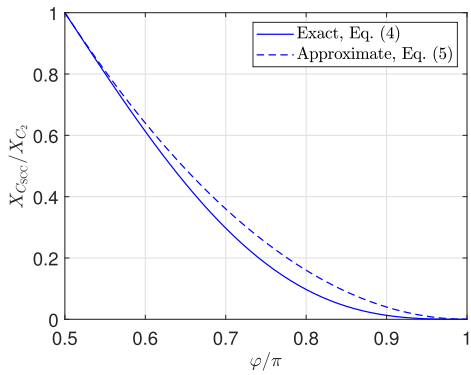

Fig. 5. Equivalent impedance $X_{C_{\text{SCC}}}$ of the SCC versus control angle φ.

$$X_{C_{\text{CSS}}} = \left(2 - \frac{2\varphi - \sin 2\varphi}{\pi}\right) X_{C_2} \tag{4}$$

$$\approx \frac{4(\varphi - \pi)^2}{\pi^2} X_{C_2} \tag{5}$$

where $X_{C_{\text{CSS}}} = -\frac{1}{\omega C_{\text{CSS}}}$ and $X_{C_2} = -\frac{1}{\omega C_2}$. The complex expression (4) can be simplified into (5) by using quadratic curve fitting. Fig. 5 shows the exact and approximate curves of $X_{C_{\text{CSS}}}$ versus the control angle φ. It can be observed that $X_{C_{\text{CSS}}}$ can be modulated from a nominal reactance X_{C_2} to zero as φ is varied from 0.5π to π.

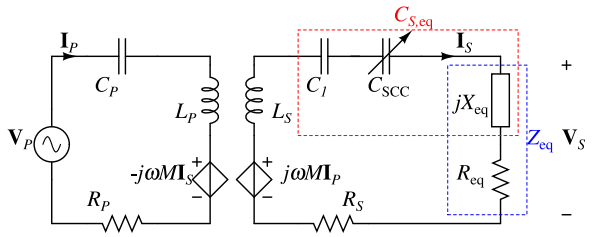

Fig. 6. AC equivalent circuit model of the proposed system.

Unless specified otherwise, in the rest of the article, $X_{\text{subscript}}$ represents the reactance of the corresponding component indicated by its subscript.

D. Equivalent Circuit Model

An equivalent circuit model of the proposed system using the fundamental approximation is shown in Fig. 6. The simplification is sufficiently accurate for resonant circuits operating near the resonant frequency [18]–[21]. Here, the equivalent circuit model of the proposed system is similar to that of a conventional SSIPT converter, except that the secondary compensation capacitance is variable and the load is not purely resistive. The load is represented by an equivalent impedance Z_{eq} with resistance R_{eq} in series with reactance X_{eq}. Variables $\mathbf{V}_P$, $\mathbf{I}_P$, $\mathbf{V}_S$, and $\mathbf{I}_S$ are phasors of the fundamental components of v_P, i_P, v_S, and i_S, respectively. Resistor R_P includes losses from the primary coil and the inverter, while resistor R_S includes losses from the secondary coil, the SCC, and the SAR. Equivalent series resistance of the the compensation capacitors can be ignored [18]–[21]. Detailed calculation of R_P and R_S will be given in Section IV-B for loss analysis.

As shown in Fig. 6, C_1, C_{SCC}, and X_{eq} donate capacitive reactances in the secondary, and they can be represented by an equivalent secondary compensation capacitance $C_{S,\text{eq}}$, with its reactance satisfying

$$X_{C_{S,\text{eq}}} = -\frac{1}{\omega C_{S,\text{eq}}} = X_{C_1} + X_{C_{\text{SCC}}} + X_{\text{eq}}. \tag{6}$$

Therefore, the equations for the circuit model in Fig. 6 are

$$(R_P + jX_{L_P} + jX_{C_P})\mathbf{I}_P - jX_M\mathbf{I}_S = \mathbf{V}_P \tag{7}$$

$$-(R_S + R_{\text{eq}} + jX_{L_S} + jX_{C_{S,\text{eq}}})\mathbf{I}_S + jX_M\mathbf{I}_P = 0 \tag{8}$$

where $X_M = \omega M$, $X_{L_P} = \omega L_P$, $X_{C_P} = -\frac{1}{\omega C_P}$, and $X_{L_S} = \omega L_S$. The magnitudes of $\mathbf{V}_P$, $\mathbf{V}_S$, and $\mathbf{I}_S$ are given by

$$|\mathbf{V}_P| = \frac{4}{\pi}V_I \tag{9}$$

$$|\mathbf{V}_S| = \frac{4}{\pi}\sin\left(\frac{\theta}{2}\right)V_O \tag{10}$$

$$|\mathbf{I}_S| = \frac{\pi}{2}\frac{I_O}{\sin^2\left(\frac{\theta}{2}\right)}. \tag{11}$$

III. Control Scheme for CP and Maximum-Efficiency Charging

A. Maximum Efficiency

Using the circuit model, shown in Fig. 6, the efficiency can be calculated by

$$\eta = \frac{|\mathbf{I}_S|^2 R_{\text{eq}}}{|\mathbf{I}_S|^2 R_{\text{eq}} + |\mathbf{I}_S|^2 R_S + |\mathbf{I}_P|^2 R_P} = \frac{X_M^2 R_{\text{eq}}}{[(R_{\text{eq}}+R_S)^2+(X_{L_S}+X_{C_{S,\text{eq}}})^2]R_P + X_M^2(R_{\text{eq}}+R_S)}. \tag{12}$$

Given a chosen operating frequency ω, the efficiency in (12) can be maximized as

$$\eta_{\max} \approx \frac{1}{\frac{2}{\frac{X_M}{\sqrt{R_P R_S}}} + 1}, \text{if} \tag{13}$$

$$X_{L_S} + X_{C_{S,\text{eq}},\text{opt}} = 0 \text{ and} \tag{14}$$

$$R_{\text{eq,opt}} = X_M\sqrt{\frac{R_S}{R_P}} \tag{15}$$

with the assumptions $\frac{X_M}{\sqrt{R_P R_S}} \gg 1$ and $\frac{R_{\text{eq}}}{R_S} \gg 1$. Variables $X_{C_{S,\text{eq}},\text{opt}}$ and $R_{\text{eq,opt}}$ are the optimum values of of $X_{C_{S,\text{eq}}}$ and R_{eq} leading to maximum efficiency, respectively [29], [30], [36], [37].

From (15), the battery resistance R_L varying in a wide range, i.e., $R_L \in [R_{L,\min}, R_{L,\max}]$, should be transformed into a matched load resistance $R_{\text{eq,opt}}$ by the SAR. With (2) and (15), the conduction angle θ of the SAR is given by

$$\theta = 2\arcsin\left(\sqrt[4]{\frac{R_{\text{eq,opt}}}{\frac{8}{\pi^2}R_L}}\right). \tag{16}$$

However, from (3), the change of θ also affects the load reactance X_{eq}, given by

$$X_{\text{eq}} = -R_{\text{eq,opt}}\cot\left(\frac{\theta}{2}\right). \tag{17}$$

In Fig. 7(a), the solid curve labeled with θ/π shows the change of θ with regard to R_L for optimum load resistance. Indicated by the dashed line, optimum load resistance $R_{\text{eq,opt}}$ can be achieved by controlling θ of the SAR. However, the magnitude of X_{eq} concurrently becomes larger with the decrease of θ, as shown in the solid curve labeled with $|X_{\text{eq}}|/R_{\text{eq,opt}}$. The simulation parameters are given in Table I and will be used for the rest of this article unless specified otherwise.

To ensure (14), $C_{S,\text{eq}}$ should fully compensate L_S at the operating frequency that the equivalent capacitive reactance $X_{C_{S,\text{eq}}}$ should be constant at $X_{C_{S,\text{eq}},\text{opt}} = -X_{L_S}$. Therefore, the variation of $X_{C_{S,\text{eq}}}$ caused by X_{eq} should be offset by $X_{C_{\text{SCC}}}$. With (5), (6), and (17), the control angle φ of the SCC can be derived as

$$\varphi \approx \pi - \frac{\pi}{2}\sqrt{\frac{|X_{C_{S,\text{eq}},\text{opt}}| - |X_{C_1}| - |X_{\text{eq}}|}{|X_{C_2}|}}. \tag{18}$$

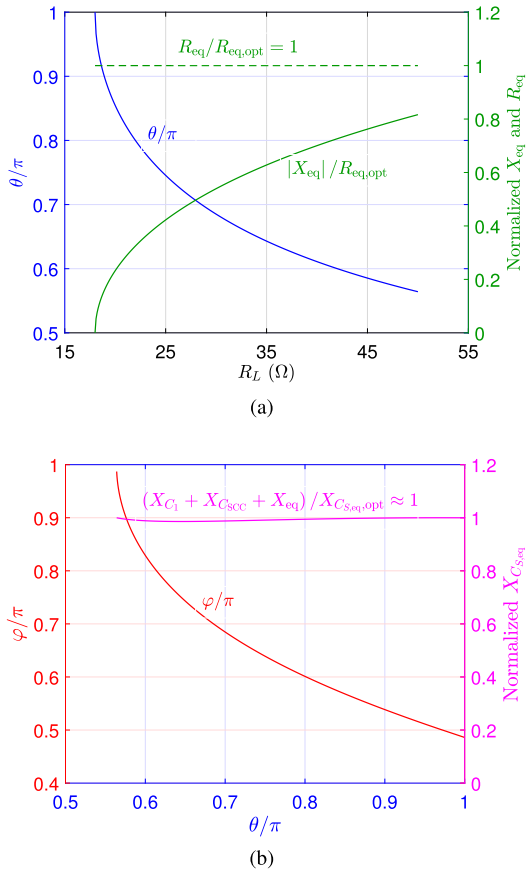

Fig. 7. (a) Conduction angle θ, normalized $R_{\rm eq}$, normalized $X_{\rm eq}$ versus load resistance R_L. (b) Phase delay angle φ, normalized $X_{C_{S,\rm eq}}$ versus conduction angle θ.

TABLE I
SIMULATION PARAMETERS

Parameters	Symbols	Values
Self inductance	L_P, L_S	86 μH, 102 μH
Coupling coefficient	k	0.26
Coil resistance	$R_{P,w}$, $R_{S,w}$	0.3 Ω, 0.328 Ω
Inverter switch	$R_{\rm on1}$	0.1 Ω
SCC switch	$R_{\rm on2}$, $V_{\rm f2}$	0.1 Ω, 0.7 V
SAR switch	$R_{\rm on3}$, $V_{\rm f3}$	0.1 Ω, 0.7 V
Operating frequency	$\frac{\omega}{2\pi}$	85 kHz
Compensation capacitance	C_P, C_1, C_2	40.8 nF, 44 nF, 166 nF
Optimum load resistance	$R_{\rm eq,opt}$	fixed at 18 Ω

As shown in Fig. 7(b), with the coordinated control of φ with respect to θ given in red curve, $X_{C_{S,\rm eq}}$ is almost constant at $X_{C_{S,\rm eq,opt}}$ achieving maximum efficiency given in magenta curve.

B. CP Charging

Equations (14) and (15) can be satisfied via controlling the conduction angle θ of the SAR and the control angle φ of the SCC, as discussed in Section III-A. As shown in Fig. 8, with the controlled optimum load resistance $R_{\rm eq,opt}$ and null reactance in the secondary, i.e., $X_{L_S}+X_{C_{S,\rm eq,opt}}=0$, the maximum efficiency, given by (13), can be maintained over a wide range of battery resistance R_L. Besides, it has been widely studied that

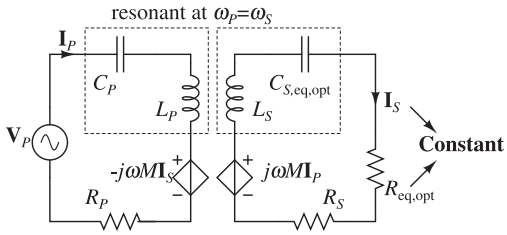

Fig. 8. Proposed operation approach to CP output and maximum efficiency with the merits of load-independent characteristic and load impedance matching.

an SSIPT system can achieve load-independent output current, if operating with a null reactance in the primary [20], [22], [23]. Theoretically, if component losses are neglected, the magnitude of the load-independent output current i_S is highlighted as

$$|\mathbf{I}_S|\approx\frac{|\mathbf{V}_P|}{X_M}. \tag{19}$$

Therefore, with the merits of load-independent transfer characteristic and load impedance matching, a novel operation approach for CP output and maximum efficiency is proposed, as illustrated in Fig. 8. The magnitude of the output current is constant at $|\mathbf{I}_S|$ due to the native load-independent current transfer characteristic [20], [22], [23], while the matching load for maximum efficiency is maintained constant at $R_{\rm eq,opt}$ via control. Therefore, given an input voltage, the proposed system outputs a constant output power at maximum efficiency, given by

$$P_{O,\rm constant}\approx|\mathbf{I}_S|^2_{\rm rms}\,R_{\rm eq,opt} \tag{20}$$

where subscript rms represents the calculation of rms value of the corresponding variable.

With (9)–(11), (19), and (20), the charging power, dc charging voltage, and dc charging current can be, respectively, designed with

$$P_{O,\rm constant}=\frac{8}{\pi^2}\frac{V_I^2}{\omega M}\sqrt{\frac{R_S}{R_P}} \tag{21}$$

$$V_O=\frac{V_I}{\sin^2(\frac{\theta}{2})}\sqrt{\frac{R_S}{R_P}} \tag{22}$$

$$I_O=\frac{8}{\pi^2}\frac{V_I}{\omega M}\sin^2\left(\frac{\theta}{2}\right) \tag{23}$$

C. Secondary Impedance Control Schemes

From (2), the equivalent load resistance $R_{\rm eq}$ can be modulated to the optimum value $R_{\rm eq,opt}$ by controlling the conduction angle θ. Assuming that the equivalent load impedance $X_{\rm eq}$ can be offset by the proper control of SCC impedance $X_{C_{\rm SCC}}$, the output power P_O is solely determined by the equivalent load resistance $R_{\rm eq}$, given by $P_O\approx|\mathbf{I}_S|^2_{\rm rms}R_{\rm eq}$. With (2), P_O takes a monotonic relationship with the control variable θ. As an illustration, monotonic curves of P_O versus θ for various values of battery resistance R_L are shown in Fig. 9. It can be observed that, when P_O is constant at $P_{O,\rm constant}$ in (20), the proposed system operates at its optimized efficiency. Therefore, a simple

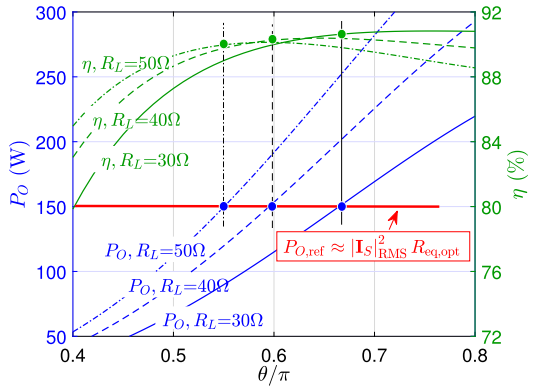

Fig. 9. Output power P_O and efficiency η versus conduction angle θ under different values of battery resistance R_L.

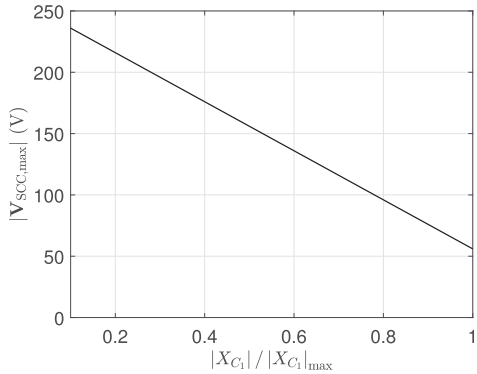

Fig. 11. Voltage stress $|\mathbf{V}_{\text{SCC,max}}|$ of the SCC versus design value of X_{C_1}.

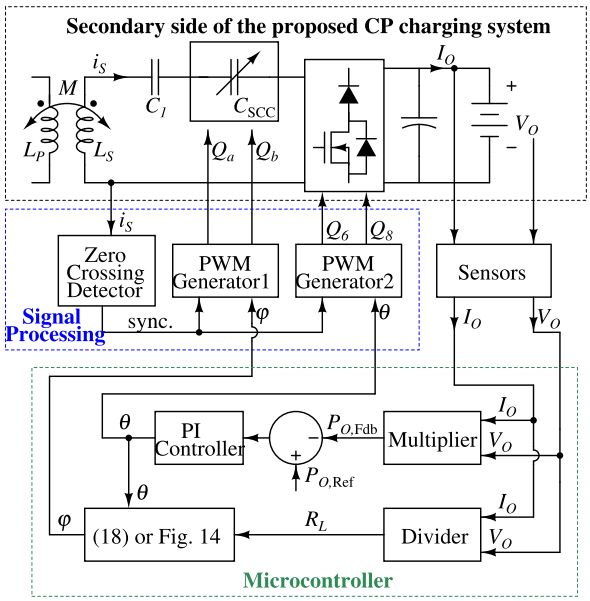

Fig. 10. Secondary impedance control diagram of the proposed CP charging system.

PI controller can be used to achieve constant output power and maintain maximum efficiency, with $P_{O,\text{constant}}$ in (20) being a control reference.

Fig. 10 shows the control diagram in practical implementation. Since the operating frequency in the primary is fixed, and only impedance control in the secondary is needed for CP output and maximum efficiency, wireless feedback communication between the primary and the secondary can be eliminated. The charging voltage V_O and the charging current I_O are measured by sensors. P_O and R_L can be calculated by a multiplier and a divider, respectively. A simple PI controller applies the correction to the difference between P_O and $P_{O,\text{ref}}$, and forms a control signal θ for the SAR. Meanwhile, with θ and R_L, another control signal φ is generated according to the analytical relationship given in (18), or alternatively, the measured relationship, such as Fig. 14. If there is no misalignment issue, both results are fine for the control. However, if there is occurrence of misalignment, (18) is more generally applicable. Zero-crossing detection of i_S generates a synchronization signal for the pulsewidth modulation (PWM) generations. Angles φ and θ are used to produce PWM driving signals for the SCC and SAR, respectively.

IV. Design Considerations

A. Minimizing Voltage Stress of the SCC

As analyzed in Sections II-B and II-C, $|X_{\text{eq}}|$ ranges from $|X_{\text{eq}}|_{\min}$ to $|X_{\text{eq}}|_{\max}$ depending on the battery resistance R_L, and $|X_{C_{\text{SCC}}}|$ ranges from zero to $|X_{C_2}|$ with the control angle φ varying from π to 0.5π. Subscripts "max" and "min" represent the maximum and minimum values of corresponding variables, respectively. $X_{C_{\text{SCC}}}$ can be controlled to offset the variation of X_{eq}, and thus, $X_{C_{S,\text{eq}}}$ can be constant at $X_{C_{S,\text{eq}},\text{opt}}$ to fully compensate X_{L_S}. From (14), design of C_1 should first ensure the requirements of full compensation in the secondary, given as

$$|X_{C_1}| + |X_{C_2}| + |X_{\text{eq}}|_{\min} \geq \left|X_{C_{S,\text{eq}},\text{opt}}\right| \text{ and} \tag{24}$$

$$|X_{C_1}| + |X_{\text{eq}}|_{\max} \leq \left|X_{C_{S,\text{eq}},\text{opt}}\right|. \tag{25}$$

The voltage stress of the SCC switches is determined by the maximum voltage across the SCC, as given by

$$|\mathbf{V}_{\text{SCC,max}}| = |X_{C_2}|\,|\mathbf{I}_S|. \tag{26}$$

To reduce the voltage stress of the SCC switches, $|X_{C_2}|$ should be minimized. In other words, with (24), we should maximize $|X_{C_1}|$ in the design. With (25), the maximum value of $|X_{C_1}|$ can be derived as

$$|X_{C_1}|_{\max} = \left|X_{C_{S,\text{eq}},\text{opt}}\right| - |X_{\text{eq}}|_{\max}. \tag{27}$$

The black curve in Fig. 11 shows the relationship between the voltage stress $|\mathbf{V}_{\text{SCC,max}}|$ and the design value of $|X_{C_1}|$. It can be observed that, the voltage stress is significantly reduced by designing a large $|X_{C_1}|$. Specifically, $|X_{C_1}| = |X_{C_1}|_{\max}$ is suggested.

Moreover, when the control angle is maximum, i.e., $\varphi = \pi$, $C_{S2,\text{eq}}$ is shorten by the switches Q_a and Q_b, and thus, maximum current stress of the SCC switches happens. Since i_S is constant as (19), maximum current stress of the SCC switches is

given by

$$|\mathbf{I}_{\mathrm{SCC,max}}| = |\mathbf{I}_S|\,. \tag{28}$$

B. Loss Analysis

Theoretically, the proposed system operates with zero phase angle between the input voltage v_P and the input current i_P. In practice, the input impedance can be designed to be slightly inductive to facilitate ZVS of the MOSFET switches Q_1–Q_4 for switching loss reduction. A slight decrement of ω_P can fulfill the requirement and will not affect the output and the efficiency too much [22], [23]. Therefore, R_P representing the primary-side losses can be estimated by considering the primary-side coil resistance and the conduction losses of the inverter switches, given by

$$R_P = R_{P,w} + 2R_{\mathrm{on},1} \tag{29}$$

where $R_{\mathrm{on},1}$ is the conduction resistance of the inverter switches Q_1–Q_4. R_P can be considered as constant.

As analyzed in Section II-C, the SCC switches Q_a and Q_b are both soft switched. The conduction loss in the SCC switches can be estimated as

$$P_{\mathrm{SCC}} = I^2_{\mathrm{SCC,rms}} R_{\mathrm{on},2} + I_{\mathrm{SCC,avg}} V_{\mathrm{f},2} \tag{30}$$

where $R_{\mathrm{on},2}$ and $V_{\mathrm{f},2}$ are the ON-resistance and body-diode forward voltage of the MOSFET switches Q_a–Q_b, respectively. $I_{\mathrm{SCC,rms}}$ and $I_{\mathrm{SCC,AV}}$ are the rms value and average value of the current flowing through the SCC switches Q_a–Q_b, given, respectively, as given by

$$I_{\mathrm{SCC,rms}} = \sqrt{\frac{1}{\pi}\int_{\pi-\varphi}^{\varphi} (|\mathbf{I}_S|\sin x)^2\, dx} \tag{31}$$

$$I_{\mathrm{SCC,avg}} = \frac{1}{\pi}\int_{\pi-\varphi}^{\varphi} |\mathbf{I}_S|\sin x\, dx. \tag{32}$$

Similarly, neglecting the small switching-OFF losses of Q_6 and Q_8, the conduction loss in the SAR can be estimated as

$$P_{\mathrm{SAR}} = i^2_{S,\mathrm{rms}} R_{\mathrm{on},3} + i_{S,\mathrm{avg}} V_{\mathrm{f},3} \tag{33}$$

where $R_{\mathrm{on},3}$ is the ON-resistance of the MOSFET switches Q_6 and Q_8, and $V_{\mathrm{f},3}$ is the forward voltage of the diodes D_5–D_8. $i_{S,\mathrm{rms}} = \frac{|\mathbf{I}_S|}{\sqrt{2}}$ and $I_{\mathrm{SAR,avg}} = \frac{2|\mathbf{I}_S|}{\pi}$ are the the rms value and average value of i_S injecting into the SAR, respectively.

Incorporating the losses in the SCC and the SAR, equivalent series resistance R_S representing the losses in the secondary-side can be calculated as

$$R_S = R_{S,w} + \frac{P_{\mathrm{SCC}} + P_{\mathrm{SAR}}}{i^2_{S,\mathrm{rms}}}. \tag{34}$$

Loss resistance ratio $\sqrt{\frac{R_S}{R_P}}$ is simulated, as shown by the blue curve in Fig. 12. Since the loss of the SCC increases with the increase of the control angle φ, $\sqrt{\frac{R_S}{R_P}}$ varies from 1.1 to 1.3 with respect to the battery resistance R_L. Theoretically, the optimum load resistance $R_{\mathrm{eq,opt}}$ should vary with the variation of $\sqrt{\frac{R_S}{R_P}}$. In practical, a slight deviation from the optimum load resistance will not affect the efficiency too much, and thus, $R_{\mathrm{eq,opt}}$ can be fixed for simplicity. The simulated efficiency shown by the green curve in Fig. 12 slightly decreases mainly due to the increase of R_S. Nevertheless, the efficiency is approximately maintained maximum over the whole load range.

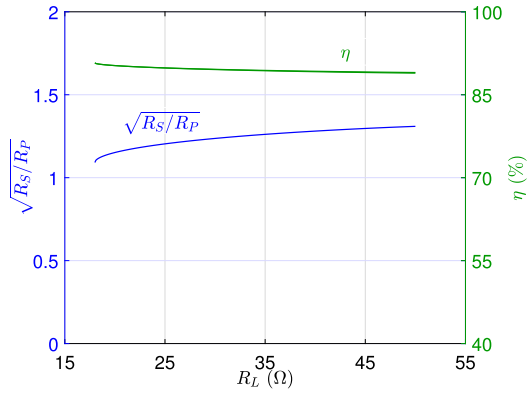

Fig. 12. Loss resistance ratio $\sqrt{\frac{R_S}{R_P}}$ and efficiency η versus equivalent battery resistance R_L.

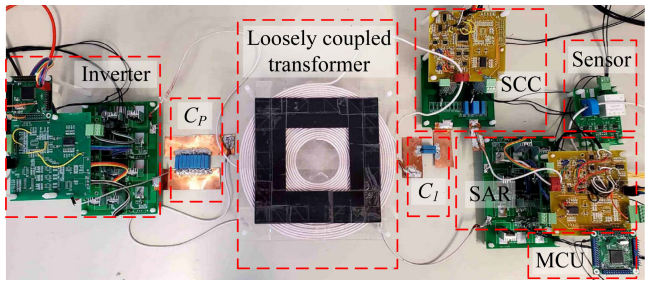

Fig. 13. Experimental setup.

V. Experimental Verification

A. Specifications and Prototype

To verify the CP output and maximum-efficiency performance throughout the charging process, an experimental prototype is built, as shown in Fig. 13. The system parameters are given in Table II. According to the charging specifications, the equivalent battery resistance approximately ranges from 18 to 50 Ω. An electronic load is used to emulate the battery. The input dc power and output dc power are measured by a Yokogawa WT1800 Precision Power Scope.

B. Measured Operating Points, Output Power, and Efficiency

The operating frequency of the inverter is fixed at 85 kHz. Following the proposed operation approach in Section III, the conduction angle θ of the SAR and the control angle φ of the SCC are adjusted to achieve CP output and maintain maximum efficiency. The measured operating points (marked with "◯") are shown in Fig. 14, with φ and θ varying from 0.53 to 0.83π and from 0.95 to 0.57π, respectively.

TABLE II
SYSTEM PARAMETERS

Battery Specifications	Values
Rated charging power P_O	150 W
Battery terminal voltage V_O	51–84.6 V

Parameters	Symbols	Measured Values
Input voltage	V_I	48 V
Switches	Q_1–Q_4, Q_a, Q_b, Q_6, Q_8	IPP60R099 with $R_{\text{on}} \approx 0.099\ \Omega$ and $V_{\text{F}} \approx 0.7$ V
Diodes	D_5, D_7	MBR20200 with $V_{\text{F}} \approx 0.7$ V
Self inductance	L_P, L_S	85.09 μH, 101.13 μH
Coupling coefficient	k	0.262
Coil resistance	$R_{P,w}$, $R_{S,w}$	0.38 Ω, 0.41 Ω
Primary compensation	C_P	41 nF
Secondary compensation	C_1, C_2	155 nF, 55nF
Operating frequency	$\frac{\omega}{2\pi}$	85 kHz

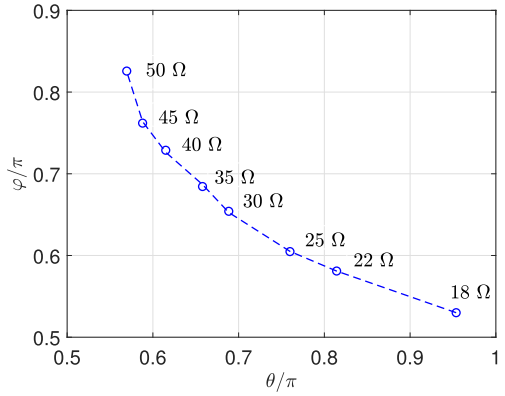

Fig. 14. Measured operating points at a constant output power of 147 W and the corresponding battery resistances.

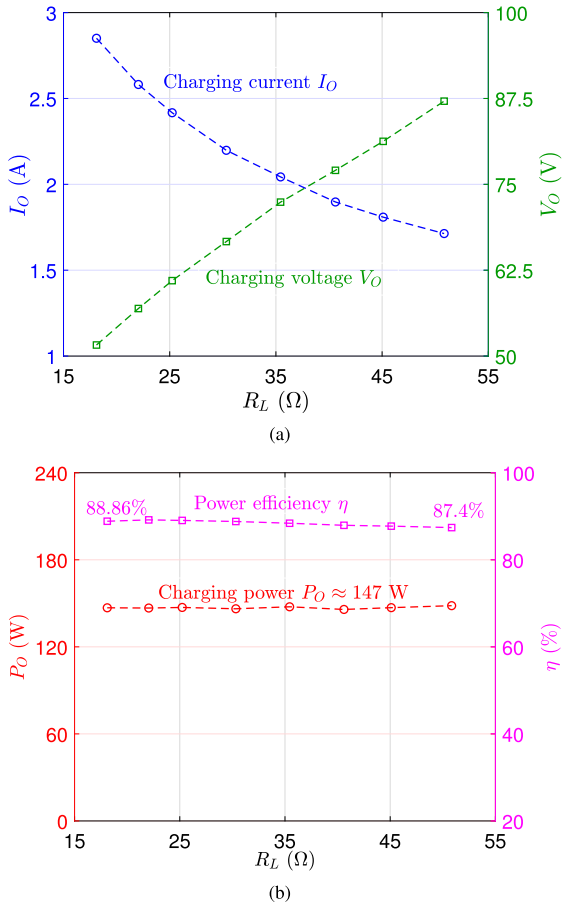

Fig. 15. (a) Measured output current and voltage versus battery resistance. (b) Measured power and efficiency versus battery resistance.

The corresponding charging current (marked with "◯") varies inversely with respect to the charging output voltage (marked with "□"), as shown in Fig. 15(a). The corresponding output power (marked with "◯") are approximately constant at 147 W, while a maximum efficiency (marked with "□") is maintained at around 88%, as shown in Fig. 15(a), which is consistent with the analysis in Section IV-B. To sum up, the proposed operation approach can ensure CP charging and maximum efficiency throughout the charging process.

Waveforms of the inverter, the SCC, and the SAR are measured at the start, middle, and end of CP charging, as shown in Fig. 16. ZVS is achievable in the inverter, SCC, and SAR. The maximum voltage stress of the SCC switches is about 55 V, as shown in Fig. 16(a), which coincides with the analysis in Section IV-A.

C. Transient Response Against Load Change

The closed-loop secondary impedance control scheme demonstrated in Section III-C is implemented in a microcontroller for CP charging and maximum efficiency throughout the charging process. Transient waveforms for step load changing are shown in Fig. 17. The output voltage V_O and output current I_O are measured and shown as CH7 in blue and CH8 in green, respectively. The control variables are observed from digital-to-analog outputs, where CH9 in red and CH11 in magenta represent the conduction angle θ of the SAR and the control angle φ of the SCC, respectively. P_O is calculated by multiplying V_O and I_O and shown as the waveform in yellow. It can be observed that P_O is tightly regulated by direct control of θ, while φ is coordinately controlled with the variation of θ and R_L. No wireless communication is needed for the control of the proposed system.

D. Discussion on Misalignment Issue

For stationary IPT charging applications, the coupling coefficient is commonly fixed once the positioning process is finished, and it will rarely fluctuate during the charging process [27], [30], [32]. Although misalignment may occur due to low-precision positioning, variation of the coupling coefficient k is normally restricted to a small range with a proper design of the loosely coupled transformer [38]. The small variation of k slightly affects the magnitude of the load-independent output current $|\mathbf{I}_S|$ given in (28), but the output power P_O, given by $P_O \approx |\mathbf{I}_S|^2_{\text{rms}} R_{\text{eq}}$, can be directly regulated to be constant by controlling the equivalent load resistance R_{eq} via the conduction angle θ of the SAR, as shown in Figs. 9 and 10. Moreover, with (16)–(18), the control angle φ of the SCC is regardless of the variation of k and responsible for an optimum null reactance

Fig. 16. Measured operating waveforms of the inverter, the SCC, and the SAR at the (a) start $R_L = 18\ \Omega$, (b) middle $R_L = 30\ \Omega$, and (c) end $R_L = 50\ \Omega$ of CP charging.

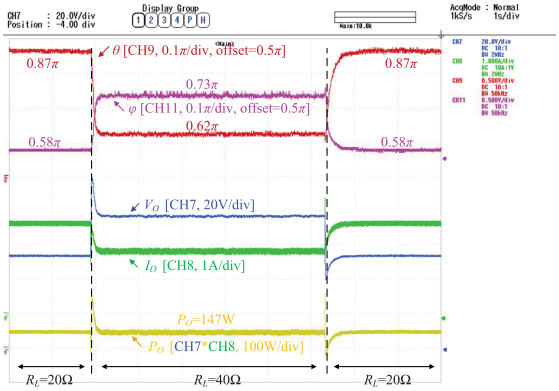

Fig. 17. Transient waveforms for R_L step changing from 20 to 40 Ω and back to 20 Ω

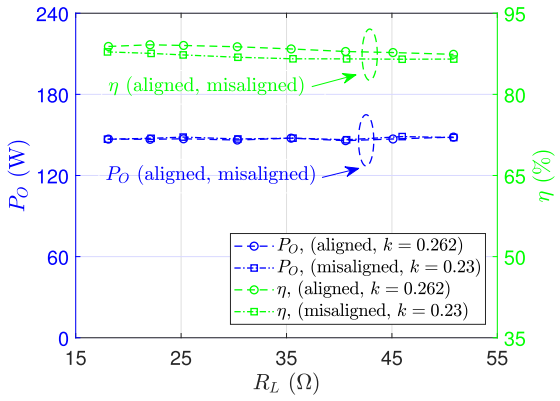

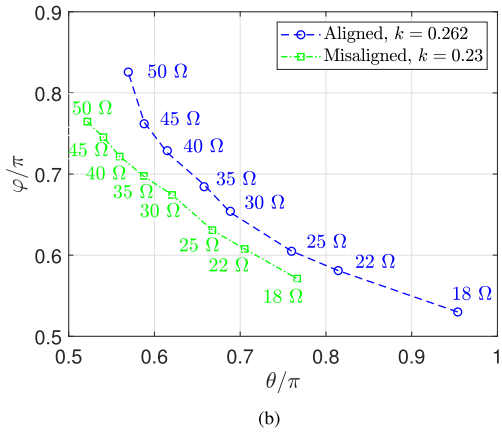

Fig. 18. Validation of the proposed method under aligned and misaligned conditions. (a) Measured output power and efficiency versus battery resistance. (b) Measured operating points.

in the secondary side, as required by (14). Therefore, even if there exists a misalignment issue, our proposed control can still ensure CP output. It should be noted that, for abnormal seriously misaligned conditions where k is extremely small, excessively large input power is required to provide the nominal CP output, and thus, overcurrent protection in the primary side should be implemented to prevent damages to the circuit.

A validation of the proposed method is conducted under aligned condition ($k = 0.262$) and misaligned condition ($k = 0.23$). An identical output power of 147 W can be ensured even if there is a misalignment, as shown in Fig. 18(a). The slight efficiency degradation is mainly brought by the reduction of k in misaligned condition. The corresponding relationships between θ and φ are given in Fig. 18(b).

VI. Conclusion

A single-stage IPT converter, which can operate as a wireless CP battery charger and maintain maximum efficiency throughout the charging process, is proposed in this article. A novel operation approach combines the merits of load-independent transfer characteristic and load impedance matching, by controlling the control angle of the SCC and the conduction angle of the SAR. The operating frequency of the IPT converter is fixed, and only a simple control in the secondary side

is employed to achieve CP output and to ensure load matching for the maximum efficiency. No wireless feedback communication is needed for the control, and all power switches realize ZVS.

REFERENCES

[1] G. A. Covic and J. T. Boys, "Inductive power transfer," *Proc. IEEE*, vol. 101, no. 6, pp. 1276–1289, Jun. 2013.

[2] S. Lukic and Z. Pantic, "Cutting the cord: Static and dynamic inductive wireless charging of electric vehicles," *IEEE Electrific. Mag.*, vol. 1, no. 1, pp. 57–64, Sep. 2013.

[3] S. Y. R. Hui and W. W. C. Ho, "A new generation of universal contactless battery charging platform for portable consumer electronic equipment," *IEEE Trans. Power Electron.*, vol. 20, no. 3, pp. 620–627, May 2005.

[4] S. Y. Hui, "Planar wireless charging technology for portable electronic products and Qi," *Proc. IEEE*, vol. 101, no. 6, pp. 1290–1301, Jun. 2013.

[5] Q. Chen, S. C. Wong, C. K. Tse, and X. Ruan, "Analysis, design and control of a transcutaneous power regulator for artificial hearts," *IEEE Trans. Biomed. Circuits Syst.*, vol. 3, no. 1, pp. 23–31, Feb. 2009.

[6] R. Bosshard and J. W. Kolar, "Inductive power transfer for electric vehicle charging: Technical challenges and tradeoffs," *IEEE Power Electron. Mag.*, vol. 3, no. 3, pp. 22–30, Sep. 2016.

[7] J. T. Boys and G. A. Covic, "The inductive power transfer story at the University of Auckland," *IEEE Circuits Syst. Mag.*, vol. 15, no. 2, pp. 6–27, Apr. 2015.

[8] J. Biela, U. Badstuebner, and J. W. Kolar, "Impact of power density maximization on efficiency of dc–dc converter systems," *IEEE Trans. Power Electron.*, vol. 24, no. 1, pp. 288–300, Jan. 2009.

[9] A. A. Hussein and I. Batarseh, "A review of charging algorithms for nickel and lithium battery chargers," *IEEE Trans. Veh. Technol.*, vol. 60, no. 3, pp. 830–838, Mar. 2011.

[10] J. Cao and A. Emadi, "A new battery/ultracapacitor hybrid energy storage system for electric, hybrid, and plug-in hybrid electric vehicles," *IEEE Trans. Power Electron.*, vol. 27, no. 1, pp. 122–132, Jan. 2012.

[11] M. Yilmaz and P. T. Krein, "Review of battery charger topologies, charging power levels, and infrastructure for plug-in electric and hybrid vehicles," *IEEE Trans. Power Electron.*, vol. 28, no. 5, pp. 2151–2169, May 2013.

[12] S. S. Zhang, "The effect of the charging protocol on the cycle life of a Li-ion battery," *J. Power Sources*, vol. 161, no. 2, pp. 1385–1391, Jul. 2006.

[13] D. Mishra, S. De, and K. R. Chowdhury, "Charging time characterization for wireless RF energy transfer," *IEEE Trans. Circuits Sys. II, Express Briefs*, vol. 62, no. 4, pp. 362–366, Apr. 2015.

[14] K. P. Dehnel, "Maximum power regulated battery charger," U.S. Patent 5 382 893, Jan. 17, 1995.

[15] R. Tanikawa and H. Le, "Constant power battery charger," WO1996037941A1, Nov. 28, 1996.

[16] N. K. Poon, B. M. H. Pong, and C. K. Tse, "A constant-power battery charger with inherent soft switching and power factor correction," *IEEE Trans. Power Electron.*, vol. 18, no. 6, pp. 1262–1269, Nov. 2003.

[17] U. S. Kim, J. Yi, C. B. Shin, T. Han, and S. Park, "Modeling the thermal behaviors of a lithium-ion battery during constant-power discharge and charge operations," *J. Electrochem. Soc.*, vol. 160, no. 6, pp. A990–A995, Apr. 2013.

[18] W. Zhang, S. C. Wong, C. K. Tse, and Q. Chen, "Analysis and comparison of secondary series and parallel compensated inductive power transfer systems operating for optimal efficiency and load-independent voltage transfer ratio," *IEEE Trans. Power Electron.*, vol. 29, no. 6, pp. 2979–2990, Jun. 2014.

[19] Y. H. Sohn, B. H. Choi, E. S. Lee, G. C. Lim, G. H. Cho, and C. T. Rim, "General unified analyses of two-capacitor inductive power transfer systems: Equivalence of current-source SS and SP compensations," *IEEE Trans. Power Electron.*, vol. 30, no. 11, pp. 6030–6045, Nov. 2015.

[20] W. Zhang, S. C. Wong, C. K. Tse, and Q. Chen, "Load-independent duality of current and voltage outputs of a series or parallel compensated inductive power transfer converter with optimized efficiency," *IEEE J. Emerg. Sel. Topics. Power Electron.*, vol. 3, no. 1, pp. 137–146, Mar. 2015.

[21] Z. Huang, Z. Fang, C. S. Lam, P. I. Mak, and R. P. Martins, "Cost-effective compensation design for output customization and efficiency optimization in series/series-parallel inductive power transfer converter," *IEEE Trans. Ind. Electron.*, to be published. doi: 10.1109/TIE.2019.2959491.

[22] Z. Huang, S. C. Wong and C. K. Tse, "Design of a single-stage inductive-power-transfer converter for efficient EV battery charging," *IEEE Trans. Veh. Technol.*, vol. 66, no. 7, pp. 5808–5821, Jul. 2017.

[23] X. Qu, W. Zhang, S. C. Wong, and C. K. Tse, "Design of a current-source-output inductive power transfer LED lighting system," *IEEE J. Emerg. Sel. Topics Power Electron.*, vol. 3, no. 1, pp. 306–314, Mar. 2015.

[24] H. Zeng and F. Z. Peng, "SiC-based Z-source resonant converter with constant frequency and load regulation for EV wireless charger," *IEEE Trans. Power Electron.*, vol. 32, no. 11, pp. 8813–8822, Nov. 2017.

[25] O. Knecht and J. W. Kolar, "Performance evaluation of series-compensated IPT systems for transcutaneous energy transfer," *IEEE Trans. Power Electron.*, vol. 34, no. 1, pp. 438–451, Jan. 2019.

[26] A. Berger, M. Agostinelli, S. Vesti, J. A. Oliver, J. A. Cobos, and M. Huemer, "A wireless charging system applying phase-shift and amplitude control to maximize efficiency and extractable power," *IEEE Trans. Power Electron.*, vol. 30, no. 11, pp. 6338–6348, Nov. 2015.

[27] Z. Li, C. Zhu, J. Jiang, K. Song, and G. Wei, "A 3-kW wireless power transfer system for sightseeing car supercapacitor charge," *IEEE Trans. Power Electron.*, vol. 32, no. 5, pp. 3301–3316, May 2017.

[28] W. Zhong and S. Y. Hui, "Reconfigurable wireless power transfer systems with high energy efficiency over wide load range," *IEEE Trans. Power Electron.*, vol. 33, no. 7, pp. 6379–6390, Jul. 2018.

[29] W. X. Zhong and S. Y. R. Hui, "Maximum energy efficiency tracking for wireless power transfer systems," *IEEE Trans. Power Electron.*, vol. 30, no. 7, pp. 4025–4034, Jul. 2015.

[30] Z. Huang, S. C. Wong, and C. K. Tse, "An inductive-power-transfer converter with high efficiency throughout battery-charging process," *IEEE Trans. Power Electron.*, vol. 34, no. 10, pp. 10245–10255, Oct. 2019.

[31] T. Diekhans and R. W. De Doncker, "A dual-side controlled inductive power transfer system optimized for large coupling factor variations and partial load," *IEEE Trans. Power Electron.*, vol. 30, no. 11, pp. 6320–6328, Nov. 2015.

[32] Q. Chen, L. Jiang, J. Hou, X. Ren, and X. Ruan, "Research on bidirectional contactless resonant converter for energy charging between EVs," in *Proc. 39th Annu. Conf. IEEE Ind. Electron. Soc.*, Vienna, Austria, Nov. 2013, pp. 1236–1241.

[33] K. Colak, E. Asa, M. Bojarski, D. Czarkowski, and O. C. Onar, "A novel phase-shift control of semibridgeless active rectifier for wireless power transfer," *IEEE Trans. Power Electron.*, vol. 30, no. 11, pp. 6288–6297, Nov. 2015.

[34] W. Gu and K. Harada, "A new method to regulate resonant converters," *IEEE Trans. Power Electron.*, vol. 3, no. 4, pp. 430–439, Oct. 1988.

[35] M. Yaqoob, K. Loo, and Y. M. Lai, "Fully soft-switched dual-active-bridge series-resonant converter with switched-impedance-based power control," *IEEE Trans. Power Electron.*, vol. 33, no. 11, pp. 9267–9281, Nov. 2018.

[36] T. D. Yeo, D. Kwon, S. T. Khang, and J. W. Yu, "Design of maximum efficiency tracking control scheme for closed-loop wireless power charging system employing series resonant tank," *IEEE Trans. Power Electron.*, vol. 32, no. 1, pp. 471–478, Jan. 2017.

[37] Y. Yang, W. Zhong, S. Kiratipongvoot, S. C. Tan, and S. Y. R. Hui, "Dynamic improvement of series-series compensated wireless power transfer systems using discrete sliding mode control," *IEEE Trans. Power Electron.*, vol. 33, no. 7, pp. 6351–6360, Jul. 2018.

[38] M. Budhia, G. A. Covic, and J. T. Boys, "Design and optimization of circular magnetic structures for lumped inductive power transfer systems," *IEEE Trans. Power Electron.*, vol. 26, no. 11, pp. 3096–3108, Nov. 2011.

Zhicong Huang (Member, IEEE) received the B.Eng. degree in electrical engineering and automation and the M.Phil. degree in mechanical and electronic engineering from the Huazhong University of Science and Technology, Wuhan, China, in 2010 and 2013, respectively, and the Ph.D. degree in power electronics from The Hong Kong Polytechnic University, Hong Kong, in 2018.

He is currently an Assistant Professor with the Shien-Ming Wu School of Intelligent Engineering, South China University of Technology, Guangzhou, China. In 2019, he was a Postdoctoral Fellow under the UM Macao Talent Program, with the State Key Laboratory of Analog and Mixed-Signal VLSI, University of Macau, Macao, China. His research interests include wireless power transfer, electric vehicles, and artificial intelligence.

Chi-Seng Lam (Senior Member, IEEE) received the Ph.D. degree in electrical and electronics engineering from the University of Macau (UM), Macao, China, in 2012.

He completed the Clare Hall Study Programme with the University of Cambridge, Cambridge, U.K., in 2019. From 2006 to 2009, he was an Electrical and Mechanical Engineer with UM. From 2009 to 2012, he simultaneously worked as a Laboratory Technician with UM and toward the Ph.D. degree. In 2013, he was a Postdoctoral Fellow with The Hong Kong Polytechnic University, Hong Kong. He is currently an Associate Professor with the State Key Laboratory of Analog and Mixed-Signal VLSI and Institute of Microelectronics, UM, and also with the Department of Electrical and Computer Engineering, Faculty of Science and Technology, UM. He has coauthored or coedited four books and more than 100 technical journals and conference papers. He holds four US patents and two Chinese patents. His research interests include power quality compensators, renewable energy generation, integrated power electronics controllers, power management integrated circuits, and wireless power transfer.

Dr. Lam was a recipient or corecipient of the IEEE Power and Energy Society Chapter Outstanding Engineer Award in 2016, Best Track Paper Award of the Asia-Pacific Power and Energy Engineering Conference (APPEEC) 2019, Best Paper Award of Integrated Circuits, Technologies and Applications (ICTA) 2019, Merit Paper Award of Third RIUPEEEC Conference in 2005, the Macao Science and Technology Invention Award (Second Class and Third Class), the Research and Development Award for Postgraduates (Ph.D.) in 2012, 2014, and 2018, respectively. He was a member of the Organizing Committee or Technical Program Committee of several international conferences, including the Annual Conference of the IEEE Industrial Electronics Society (IECON) 2019, Asian Solid-State Circuits Conference (ASSCC) 2019, APPEEC 2019, IECON 2018, International Conference on Industrial Electronics for Sustainable Energy Systems (IESES) 2018, Asia and South Pacific Design Automation Conference (ASP-DAC) 2016, and TENCON 2015. He was a Tutorial Speaker for APPEEC 2019. He was the Chair of IEEE Macau Circuits and Systems (CAS) Chapter from 2017 to 2018. He is currently the Vice-Chair of IEEE Macau Section and the Chair of IEEE Macau IES Chapter.

Pui-In Mak (Fellow, IEEE) received the Ph.D. degree from the University of Macau (UM), Macao, China, in 2006.

He is currently a Full Professor with the UM Faculty of Science and Technology—ECE, and the Associate Director (Research) with the UM State Key Laboratory of Analog and Mixed-Signal VLSI. His research interests include analog and radio-frequency (RF) circuits and systems for wireless and multidisciplinary innovations.

Prof. Mak was the co-receiver of the Design Automation Conference (DAC)/ International Solid-State Circuits Conference (ISSCC) Student Paper Award 2005, IEEE Circuits and Systems Society Outstanding Young Author Award 2010, National Scientific and Technological Progress Award 2011, Best Associate Editor for the IEEE TRANSACTIONS ON CIRCUITS AND SYSTEMS II from 2012 to 2013, Asian Solid-State Circuits Conference (A-SSCC) Distinguished Design Award 2015, and ISSCC Silkroad Award 2016. In 2005, he was given the Honorary Title of Value for Scientific Merits by the Macau Government. Since 2018, he has been an Overseas Expert of the Chinese Academy of Sciences. He is also a fellow of the IET. He was an Editorial Board Member of IEEE Press from 2014 to 2016 a member of the Board-of-Governors of IEEE Circuits and Systems Society from 2009 to 2011; a Senior Editor for IEEE JOURNAL ON EMERGING AND SELECTED TOPICS IN CIRCUITS AND SYSTEMS from 2014 to 2015; an Associate Editor for the IEEE JOURNAL OF SOLID-STATE CIRCUITS (since 2018), IEEE SOLID-STATE CIRCUITS LETTERS (since 2017), IEEE TRANSACTIONS ON CIRCUITS AND SYSTEMS I (2010–2011, 2014–2015), and IEEE TRANSACTIONS ON CIRCUITS AND SYSTEMS II from 2010 to 2013). He was the TPC Vice Co-Chair of Asia and South Pacific DAC (ASP-DAC) in 2016, TPC Member of A-SSCC from 2013 to 2016, European Solid-State Circuits Conference (ESSCIRC) from 2016 to 2017, and ISSCC from 2017 to 2019. He was a Distinguished Lecturer of the IEEE Circuits and Systems Society from 2014 to 2015 and IEEE Solid-State Circuits Society from 2017 to 2018. He is currently the Chair of the Distinguished Lecturer Program of IEEE Circuits and Systems Society from 2018 to 2019.

Rui Paulo da Silva Martins (Fellow, IEEE) was born on April 30, 1957. He received the bachelor's, master's, Ph.D., and Habilitation degrees in electrical engineering and computers from the Department of Electrical and Computer Engineering (DECE), Instituto Superior Técnico (IST), University of Lisbon, Lisbon, Portugal, in 1980, 1985, 1992, and 2001, respectively.

Since October 1980, he has been with the DECE/IST, University of Lisbon. Since 1992, he has been on leave from the University of Lisbon and is currently with the DECE, Faculty of Science and Technology (FST), University of Macau (UM), Macao, China, where he was the Dean of the Faculty from 1994 to 1997. From September 2008 to August 2018, he was the Vice-Rector (Research); from September 2018 to August 2023, the Vice-Rector (Global Affairs); where, since 1997, he has been the Vice-Rector with UM. Within the scope of his teaching and research activities, he has taught 21 bachelor's and master's courses and, while at UM, supervised or cosupervised 26 theses for Ph.D. and 21 theses for master's courses. He is the co-author of seven books, 11 book chapters, 32 U.S. patents, 3 Taiwanese patents, and 1 Chinese patent, 217 papers in scientific journals and 320 papers in conference proceedings, and 64 other academic works. In 2003, he created the Analog and Mixed-Signal VLSI Research Laboratory of UM, which, in January 2011, was elevated to State Key Laboratory (SKLAB) of China (the first in Engineering in Macao), and is its Founding Director. From January 2009 to March 2019, he was the Founding Chair of UMTEC (UM company), supporting the incubation and creation in 2018 of Digifluidic, the first UM Spin-Off, whose CEO is an SKLAB Ph.D. graduate. He was also a Co-Founder of Chipidea Microelectronics (Macao) (now Synopsys-Macao) during 2001–2002.

Prof. Martins was the recipient of two Macao Government decorations: the Medal of Professional Merit (Portuguese, 1999) and the Honorary Title of Value (Chinese, 2001). He was also the recipient of the IEEE Council on Electronic Design Automation (CEDA) Outstanding Service Award in 2016 and was also nominated Best Associate Editor during 2012–2013. He was the Founding Chair of IEEE Macau Section from 2003 to 2005 and IEEE Macau Joint-Chapter on Circuits and Systems (CAS)/Communications (COM) from 2005 to 2008 [2009 World Chapter of the Year of IEEE CAS Society (CASS)], General Chair of IEEE Asia-Pacific Conference on CAS (APCCAS2008), Vice-President (VP) of Region 10 (Asia, Australia, and Pacific) from 2009 to 2011 and VP of World Regional Activities and Membership of IEEE CASS from 2012 to 2013, and Associate Editor for the IEEE TRANSACTIONS ON CAS II: EXPRESS BRIEFS from 2010 to 2013. He was also a member of IEEE CASS Fellow Evaluation Committee (2013, 2014, 2018-Chair, and 2019); IEEE Nominating Committee of Division I Director (CASS/EDS/SSCS) (2014); and IEEE CASS Nominations Committee during 2016–2017. In addition, he was the General Chair of ACM/IEEE Asia South Pacific Design Automation Conference ASP-DAC2016. He was also the Vice-President and the President of the Association of Portuguese Speaking Universities (AULP) from 2005 to 2014 and from 2014 to 2017, respectively. In July 2010, he was elected, unanimously, as a Corresponding Member of the Lisbon Academy of Sciences, being the only Portuguese Academician working and living in Asia.

Siu-Chung Wong (Senior Member, IEEE) received the B.Sc. degree in physics from the University of Hong Kong, Hong Kong, in 1986, the M.Phil. degree in electronics from the Chinese University of Hong Kong, Hong Kong, in 1989, and the Ph.D. degree from the University of Southampton, Southampton, U.K., in 1997.

In 1988, he joined The Hong Kong Polytechnic University, Hong Kong, as an Assistant Lecturer. He is currently an Associate Professor with the Department of Electronic and Information Engineering, The Hong Kong Polytechnic University, where he conducts research in power electronics. From 2012 to 2015, he was a Chutian Scholar Chair Professor with the Hubei Provincial Department of Education, China, and the appointment was hosted by the Wuhan University of Science and Technology, Wuhan, China. In 2013, he was a Guest Professor with the School of Electrical Engineering, Southeast University, Nanjing, China. He was a Visiting Scholar with the Center for Power Electronics Systems, Virginia Tech, VA, USA, in November 2008, Aero-Power Sci-tech Center, Nanjing University of Aeronautics and Astronautics, Nanjing, China, in January 2009, and the School of Electrical Engineering, Southeast University, Nanjing, China, in March 2012.

Dr. Wong is a member of the Electrical College, The Institution of Engineers, Australia. He is an Editor for the *Energy and Power Engineering Journal* and a member of the Editorial Board of the *Journal of Electrical and Control Engineering*. He is a Guest Associate Editor for the IEEE JOURNAL OF EMERGING AND SELECTED TOPICS IN POWER ELECTRONICS, Special Issue on "Power Electronics for Biomedical Applications," 2014 and an Associate Editor for the IEEE TRANSACTIONS ON CIRCUITS AND SYSTEMS II.

Chi K. Tse (Fellow, IEEE) received the B.Eng. degree with first class honors in electrical engineering and the Ph.D. degree from the University of Melbourne, Melbourne, VIC, Australia, in 1987 and 1991, respectively.

He is currently a Chair Professor of Electrical Engineering with the City University of Hong Kong, Hong Kong. Prior to joining the City University of Hong Kong, he was with the Hong Kong Polytechnic University, where he was the Head of the Department of Electronic and Information Engineering from 2005 to 2012. His research interests include power electronics, nonlinear systems, and complex network applications.

Dr. Tse was the recipient of a number of research and industry awards, including Prize Paper Awards by the IEEE TRANSACTIONS ON POWER ELECTRONICS in 2001, 2015, and 2017, the Best Paper Award by the *RISP Journal of Signal Processing* in 2014, the Best Paper Award by the *International Journal of Circuit Theory and Applications* in 2003, two Gold Medals at the International Inventions Exhibition in Geneva in 2009 and 2013, a Silver Medal at the International Invention Innovation Competition in Canada in 2016, a Grand Prize and Gold Medal at Silicon Valley International Inventions Festival in USA in 2019, and a number of recognitions by the academic and research communities, including honorary professorship by several Chinese and Australian universities, Chang Jiang Scholar Chair Professorship, IEEE Distinguished Lectureship, Distinguished Research Fellowship by the University of Calgary, Gledden Fellowship, and International Distinguished Professorship-at-Large by the University of Western Australia. He was also the recipient of the President's Award for Outstanding Research Performance twice, the Faculty Research Grant Achievement Award twice, the Faculty Best Researcher Award, and several teaching awards while with the Hong Kong Polytechnic University. He was the Editor-in-Chief of the IEEE TRANSACTIONS ON CIRCUITS AND SYSTEMS II (from 2016 to 2019), IEEE CIRCUITS AND SYSTEMS MAGAZINE (from 2012 to 2015), an Associate Editor for three IEEE journal/transactions, an Editor of the *International Journal of Circuit Theory and Applications*, and is on the Editorial Boards of a few other journals. Since 2007, he has been the Editor-in-Chief of the IEEE CIRCUITS AND SYSTEMS SOCIETY NEWSLETTER. He is currently the Chair of the steering committee for the IEEE TRANSACTIONS ON NETWORK SCIENCE AND ENGINEERING. He is also a Panel Member of Hong Kong Research Grants Council, and member of several professional and government committees.